

## Nonlinear Evolution of Ablation-Driven Rayleigh-Taylor Instability

R. L. McCrory

*Laboratory for Laser Energetics, University of Rochester, Rochester, New York 14623*

and

L. Montierth, R. L. Morse, and C. P. Verdon<sup>(a)</sup>

*Department of Nuclear Engineering, University of Arizona, Tucson, Arizona 85721*

(Received 5 November 1980)

Simulations of the Rayleigh-Taylor instability of ablatively accelerated thin-shell fusion targets show that the nonlinear evolution exhibits spike amplitude saturation due to ablative mass removal; the shell anterior surface evolves to a laminar (nonturbulent) quasi-stationary distorted state. The perturbed flow causes a significant departure from spherically symmetric behavior, but the laminar shell interior structure makes it appear possible to retain some of the advantages of larger-aspect-ratio fusion targets.

PACS numbers: 52.50.Jm, 47.20.+m, 52.35.Py, 52.65.+z

Spherically symmetric calculations of the behavior of laser-driven fusion targets have demonstrated major advantages of employing ablatively imploded spherical shells for obtaining optimum performance. The use of shells, as opposed to solid spheres, has been shown to reduce significantly the peak laser power required to drive successfully a target of fixed mass. In general, it is predicted that performance improves with increasing shell aspect ratio,  $A$  ( $\equiv r/\Delta r$ ), where  $r$  and  $\Delta r$  are the initial radius and thickness of the shell,<sup>1-3</sup> and the useful range of  $A$  is approximately  $5 < A < 100$ . Unfortunately, the continuous inward acceleration of a spherical shell by ablation pressure applied to its outside surface causes an instability which is a form of the Rayleigh-Taylor instability<sup>4</sup> and is capable of disrupting the spherical symmetry and subsequent thermonuclear burn enough to constitute failure. Extrapolations of linear stability theory predict failure in shells with  $A$  larger than some number near 5.<sup>1,3,5</sup> To make quantitative predictions of failure, we present nonlinear ablative calculations which show important departures from the classical nonlinear development of the instability.<sup>6-8</sup> In particular, it is seen that (1) growth of the spikes tends to saturate, i.e., their growth rate decreases significantly at large amplitude and in some cases the spike structure becomes approximately stationary except for time-dependent ablative mass-removal effects; (2) the spike structure resembles the classical case with an Atwood number,  $\alpha = 1$ ,<sup>7</sup> in the sense that no Kelvin-Helmholtz structure is seen<sup>7,8</sup>; and (3) the flow is sufficiently distorted to cause significant departure from spherically symmetric behavior but exhibits a laminar (nonturbulent) structure. The results

suggest the upper limit imposed by instability on the range of aspect ratios that can be used successfully may be extended to higher values than previously believed. Target reoptimization calculations will be required which consider the instability distortions and include the effects of converging geometry.

We study the nonlinear effects of the instability in a series of numerical simulations of a segment of a plane slab of fully ionized,  $Z=6$  material accelerated between two rigid, parallel slip surfaces by ablation pressure. The ablation is driven by a constant absorbed laser irradiance in the range  $I = 2 \times 10^{14}$  to  $10^{15}$  W/cm<sup>2</sup>, deposited at a critical density of  $n_e = 10^{21}$  cm<sup>-3</sup>. These simulations could have been done in spherical geometry (finite  $A$ ) instead of in planar geometry ( $A \rightarrow \infty$ ), but planar geometry avoids the choice of a particular  $A$  and makes identification of basic phenomena easier by eliminating convergence effects. The simulations were done with a two-dimensional (2D) triangular Lagrangian hydrodynamics code, DAISY, which includes nonlinear electron thermal conduction. The simulations employ 72 zones per perturbation wavelength. The resulting resolution is consistent with that required in recent Lagrangian simulations of the Rayleigh-Taylor instability of an incompressible inviscid fluid.<sup>7</sup>

The simulations were begun with an initially uniform shell density of 2 g/cm<sup>3</sup> and thickness of 3  $\mu$ m, and run until a quasisteady ablative flow is established near the shell surface. At this time,  $t_I$ , the simulation is made 2D, and the instability is initialized by imposing a divergence-free perturbation of the form  $\xi^{\vec{r}} = \nabla \times (\hat{z} A_z)$ ,  $A_z = (\xi_0/k_y) \sin(k_y y) \operatorname{sech}[k_y(x - x_m)]$ . Here  $x$  is the

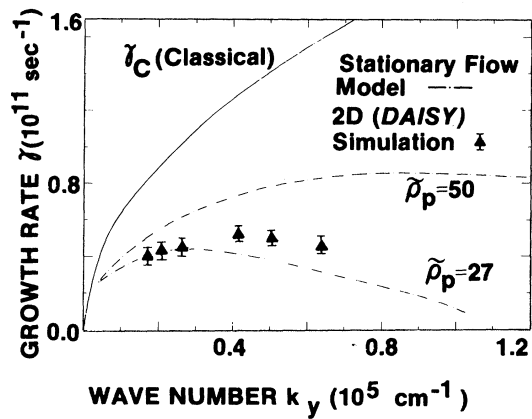


FIG. 1. Comparison of the 2D simulations of Rayleigh-Taylor linear instability growth rates with the stationary-flow model.

direction of slab motion,  $y$  runs parallel to the slab, and  $x_m$  is the point of maximum shell density. The unperturbed calculations show that the slab would be consumed by ablative mass removal at a burnthrough time of about  $t_B = 140$  psec.

To determine which unstable cases are most interesting, linear instability growth rates  $\gamma(k_y)$  were obtained from the planar stationary flow model of ablation<sup>9,10</sup> and compared with the 2D simulation results. In the 2D calculation the initialization procedure described above was used with  $\xi_0/\lambda_y = 0.01$ . Figure 1 shows a set of values of  $\gamma(k_y)$  obtained with the 2D code from an  $I = 10^{15}$  W/cm<sup>2</sup> zeroth-order solution initialized at  $t_I$ , and  $\gamma(k_y)$  obtained from the stationary model.<sup>10</sup> The stationary solutions are characterized by a single parameter, the ratio of maximum density to the isothermal sonic-point density  $\tilde{\rho}_p$ . The simulated results are not quite stationary but correspond closely to values of  $\tilde{\rho}_p \sim 27$  and are bounded by  $27 \lesssim \tilde{\rho}_p \lesssim 50$  (see Fig. 1). For comparison the classical growth rates,  $\gamma_c \equiv (k_y g)^{1/2}$  are shown. Ablative effects cause  $\gamma(k_y)$  to reach a maximum and then decrease to zero with increasing  $k_y$ , in contrast with  $\gamma_c$  which increases indefinitely (Fig. 1).<sup>1,11</sup> This result is consistent with previous time-dependent perturbation solutions.<sup>1,12</sup> The potentially troublesome and interesting range of  $k_y$  is near the maximum of  $\gamma(k_y)$  and near the inverse of the shell thickness. The case  $I = 10^{15}$  W/cm<sup>2</sup> and  $k_y = 2.5 \times 10^4 \text{ cm}^{-1}$  ( $\lambda_y = 2.5 \mu\text{m}$ ) is seen from Fig. 1 to be near the maximum, and was chosen, together with the  $k_y = 6.2 \times 10^4 \text{ cm}^{-1}$  ( $\lambda_y = 1.0 \mu\text{m}$ ) case, to study the nonlinear development of the instability.

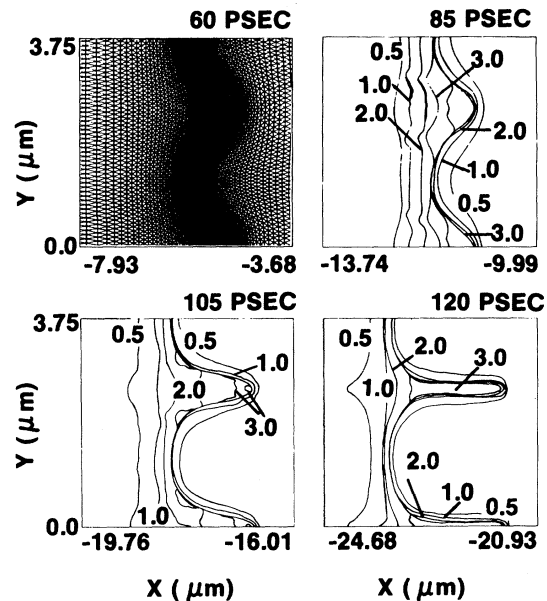


FIG. 2. Initial mesh configuration at 60 psec ( $k_y \xi_0 = \pi/5$ ) and time evolution of the density contours for the  $I = 10^{15}$  W/cm<sup>2</sup>,  $\lambda_y = 2.5 \mu\text{m}$  case.

Figure 2 shows a time sequence of density contours from a run which began with the initialization shown in the first frame ( $k_y \xi_0 = \pi/5$ ). This amplitude-to-wavelength ratio is one for which linear stability analysis is initially valid.<sup>7,8</sup> As the amplitude increases, structure is seen which resembles the classical Rayleigh-Taylor "bubble and spike"<sup>6-8</sup> phenomena, but unlike the classical behavior, the spike does not grow indefinitely because of ablative mass removal. This is also seen in the sequence of contours (Fig. 3), from the 1- $\mu\text{m}$  run. In Fig. 4, a superposition of  $\rho = 2$  g/cm<sup>3</sup> contours for the case of Fig. 3 is shown. The  $\rho = 2$  g/cm<sup>3</sup> contour was chosen to represent the approximate position of the shell surface (ablation front) because the density gradients are largest in the neighborhood of this density. Figure 5 gives the amplitude time history of the surface distortion (defined as the separation between the bubble and the spike for the  $\rho = 2$  contours). In Fig. 5, a period of exponential growth (from about 70 to 95 psec) is followed by decreased growth at an amplitude slightly less than the wavelength, followed (for the 1- $\mu\text{m}$  case) by a decrease to a smaller amplitude until burnthrough (about 140 psec). From Fig. 4 it is seen that as the spike approaches its maximum amplitude it becomes more narrow near the tip and then broadens again as its amplitude decreases while the bottom of the

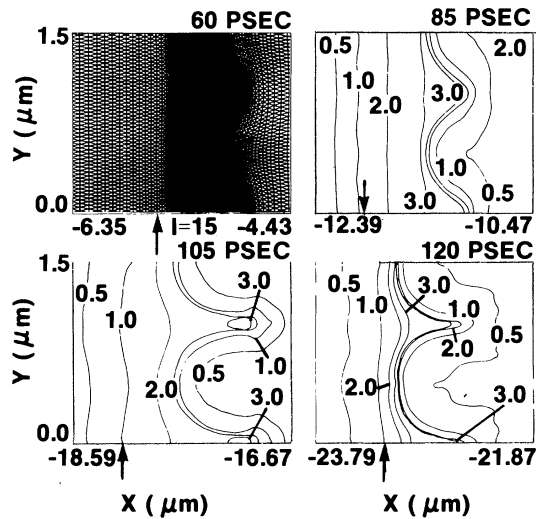


FIG. 3. Initial mesh configuration at 60 psec ( $k_y \xi_0 = \pi/5$ ) and time evolution of the density contours for the  $I = 10^{15}$  W/cm<sup>2</sup>,  $\lambda_y = 1.0 \mu\text{m}$  case.

bubble is seen to become progressively flatter. Figure 5 also illustrates the relative thickness of the shell at its thinnest region (top of the bubble) for the two unstable cases, together with the unperturbed ablated shell thickness. The 2.5- $\mu\text{m}$  case is the most globally disruptive. In examining Figs. 2 and 3, it is interesting that a quasistationary distorted state does not evolve into a further state of turbulent mixing.<sup>13</sup> The cause of the saturated amplitude of the spike is seen to be the higher ablation pressure near the tip caused by the higher temperature there than at the same density in the bubble. Contour plots of temperature (not included) show this difference. The temperatures near the tip are larger because the tips are nearer to the heat source (the critical surface is located outside and to the right of the contour plots). Interestingly, the simulations show that the center-of-mass motion of the shell is virtually unchanged by the presence of the unstable Rayleigh-Taylor flow. The disruptive nature of the instability is apparent from Fig. 5. The instability evolves because of a nearly constant bubble rise velocity which removes mass from the bubble region. Particle paths from the simulations (not illustrated) indicate that the shell thickness near the bubble decreases linearly with time. The laminar nature of the flow is illustrated by the time-independent ordering of the density contours (Figs. 2 and 3).

We summarize by noting that the form that the modes have acquired (last frames of Figs. 2 and 3) are sufficiently distorted to be a potential

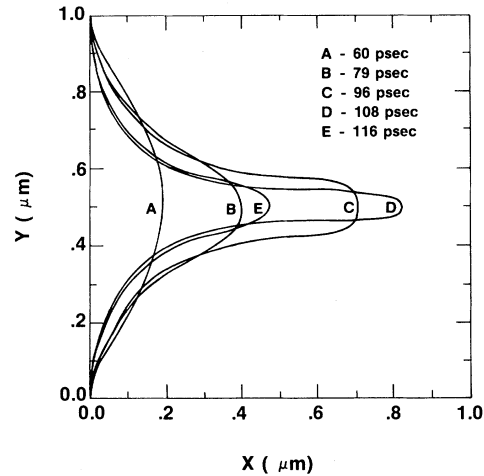


FIG. 4. Spike ( $\rho = 2 \text{ g/cm}^3$  contours) at various times for the instability illustrated in Fig. 3.

source of disruption of the final fuel compression of a large-aspect-ratio spherical fusion target. However, in both cases the left side of the shell, which is the side away from the laser and would correspond to the “inside” of a spherical shell, is seen to be less distorted than the outside. This laminar and only moderately distorted inner surface, while not as desirable as a perfectly flat (or spherical) surface, would in general not be mixed with lower-density fuel inside it. In Fig. 3, we illustrate this effect by marking a Lagrangian surface ( $i = 15$ ) whose position at  $t_I$  corresponds to a material density near  $0.8 \text{ g/cm}^3$  (about the density of shocked liquid DT fuel). Consequently, somewhat better final fuel compression would be expected than if the inner surface of the shell had

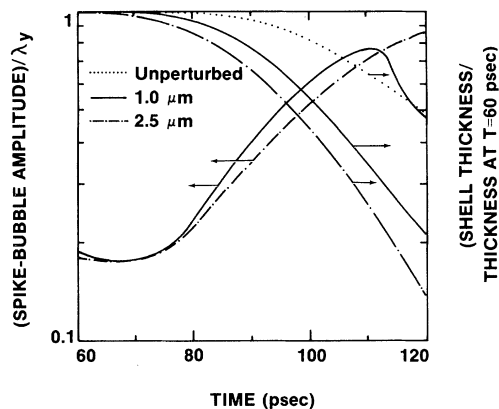


FIG. 5. Spike amplitude as a function of time for the unstable cases of Figs. 2 and 3, and shell thickness at the bubble center as a function of time for the two perturbed cases compared with the unperturbed simulation.

lost its integrity because of turbulent mixing. It therefore appears plausible that successful large-aspect-ratio inertial-confinement-fusion implosion systems may be designed to operate with shell distortions of the kind and amplitude seen here.

This work was sponsored by the Department of Energy under Contract No. DE-AC08-80DP40124 and subcontract No. 9245009 with the Lawrence Livermore National Laboratory, and by the sponsors of the Laser Fusion Feasibility Project of the Laboratory for Laser Energetics of the University of Rochester.

<sup>(a)</sup>Permanent address: Laboratory for Laser Energetics of the University of Rochester, Rochester, N. Y. 14627.

<sup>1</sup>G. Fraley, W. Gula, D. Henderson, R. McCrory, R. Malone, R. Mason, and R. Morse, in *Proceedings of the Fifth International Conference on Plasma Physics and Controlled Nuclear Fusion Research, Tokyo, Japan, 1974* (International Atomic Energy Agency, Vienna, Austria, 1974), p. 543.

<sup>2</sup>R. J. Mason, *Nucl. Fusion* **15**, 1031 (1975).

<sup>3</sup>Yu. Afanas'ev *et al.*, *Pis'ma Zh. Eksp. Teor. Fiz.* **21**,

150 (1975) [*JETP Lett.* **21**, 68 (1975)], and *Pis'ma Zh. Eksp. Teor. Fiz.* **23**, 617 (1976) [*JETP Lett.* **23**, 566 (1976)].

<sup>4</sup>S. Chandrasekhar, *Hydrodynamic and Hydromagnetic Stability* (Oxford Univ. Press, Oxford, England, 1961), Chap. 10.

<sup>5</sup>R. L. McCrory and R. L. Morse, *Phys. Fluids* **19**, 175 (1976).

<sup>6</sup>J. D. Lindl and W. C. Mead, *Phys. Rev. Lett.* **34**, 1273 (1975).

<sup>7</sup>G. R. Baker, D. I. Meiron, and S. A. Orszag, *Phys. Fluids* **23**, 1485 (1980).

<sup>8</sup>F. H. Harlow and J. E. Welch, *Phys. Fluids* **9**, 842 (1966); B. J. Daly, *Phys. Fluids* **10**, 297 (1967); J. R. Freeman, M. J. Clauser, and S. L. Thompson, *Nucl. Fusion* **17**, 223 (1977).

<sup>9</sup>S. J. Gitomer, R. L. Morse, and B. S. Newberger, *Phys. Fluids* **12**, 234 (1977).

<sup>10</sup>L. Montierth, F. L. Cochran, and R. L. Morse, *Bull. Am. Phys. Soc.* **24**, 945 (1979); R. L. McCrory, L. Montierth, R. L. Morse, and C. P. Verdon, in "Laser Interactions and Related Plasma Phenomena" (Plenum, N. Y., to be published), Vol. V.

<sup>11</sup>S. E. Bodner, *Phys. Rev. Lett.* **33**, 761 (1974).

<sup>12</sup>R. L. McCrory, R. L. Morse, and K. A. Taggart, *Nucl. Sci. Eng.* **64**, 163 (1977).

<sup>13</sup>G. Birkhoff, Los Alamos Scientific Laboratory Reports No. LA-1927, 1956 (unpublished), and No. LA-1862, 1955 (unpublished).

## Resistivity and Energy Flow in a Plasma Undergoing Magnetic-Field-Line Reconnection

N. Wild, W. Gekelman, and R. L. Stenzel

*Department of Physics, University of California at Los Angeles, Los Angeles, California 90024*

(Received 2 October 1980)

Detailed time- and space-resolved measurements of the electric fields and currents have been made in a laboratory plasma undergoing magnetic-field-line reconnection. The resistivity normalized to the classical value is found to be spatially inhomogeneous ( $10 < \eta/\eta_{cl} < 250$ ), and does not maximize in regions of large currents. Investigation of the energy balance [ $\nabla \cdot \vec{E} \times \vec{H} = -\vec{E} \cdot \vec{J} - (\partial/\partial t)(B^2/2\mu_0)$ ] shows that electron heating accounts for most of the electromagnetic energy loss.

PACS numbers: 52.25.-b, 51.60.+a

The problem of magnetic-field-line reconnection, which is important in space<sup>1,2</sup> and fusion<sup>3</sup> plasmas, is often modeled with the assumption that dissipation occurs only within a diffusion region, i.e., the neutral sheet ( $B_{\perp} \approx 0$ ). The plasma resistivity in the diffusion region determines the dissipation of magnetic field energy and the magnetic field topology. Direct measurements of resistivity and energy flow are extremely difficult to perform in space or fusion plasmas but have become possible in a controlled laboratory plasma device.<sup>4</sup>

A large-volume (1 m diam, 2 m length) highly ionized discharge plasma ( $n_e \geq 10^{12} \text{ cm}^{-3}$ ,  $kT_e \approx 5-15 \text{ eV}$ , Ar,  $2 \times 10^{-4} \text{ Torr}$ ) is bounded by two parallel-plate conductors (75 cm wide, 175 cm long, 32 cm separation) through which current (20 kA/plate) is pulsed. Both plate currents flow in the same direction (+y). In this geometry, a time varying transverse magnetic field with a vacuum x-type neutral line is produced. There is also a uniform axial dc magnetic field  $B_{y0} \approx 20 \text{ G}$ . The induced electric field ( $-\dot{A}_y \approx 1 \text{ V/cm}$ ) is parallel to the plates and in the first quarter cy-